Fig. S1

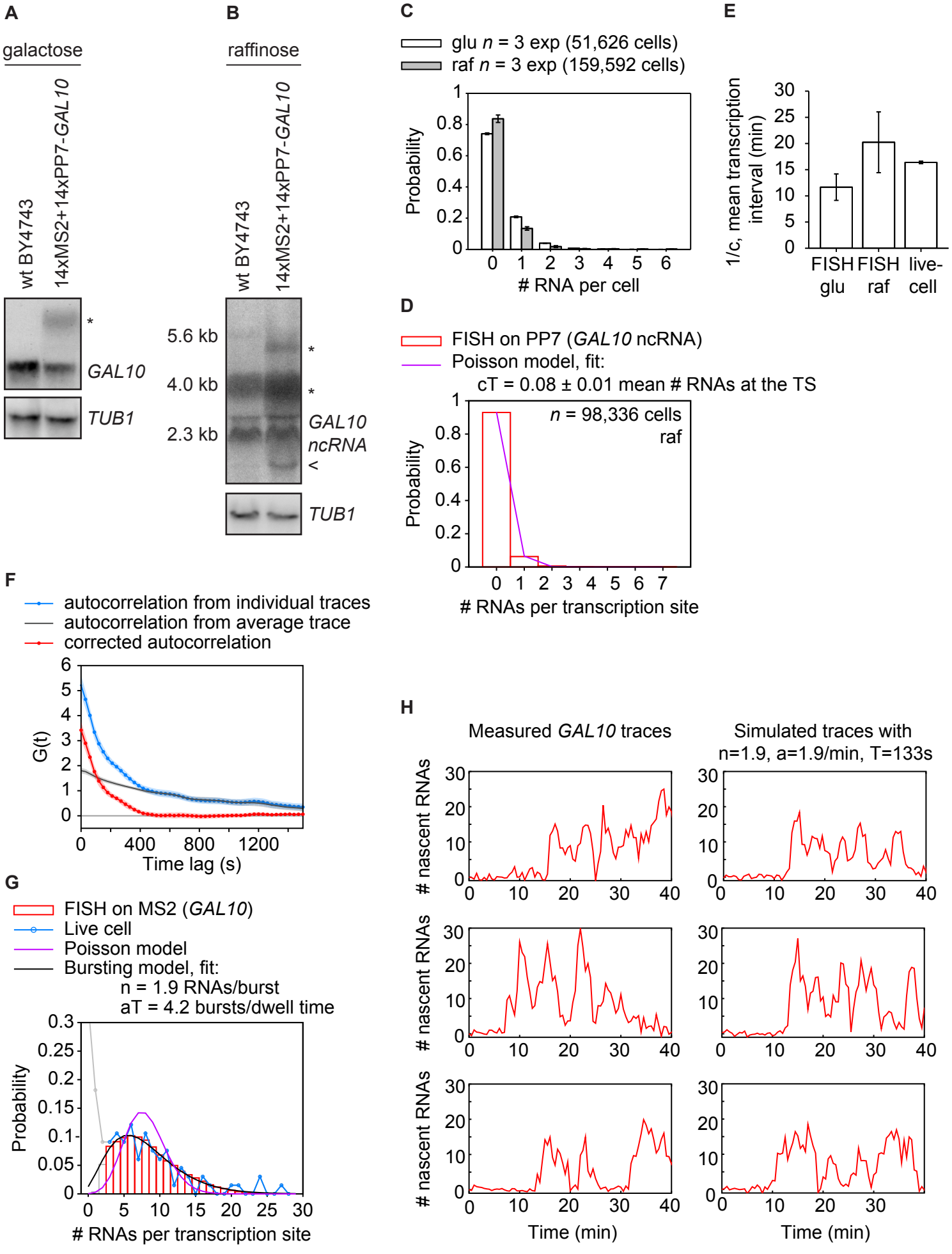
A
galactose
wt BY4743
14xMS2+14xPP7-GAL10
*
GAL10
TUB1
B
raffinose
wt BY4743
14xMS2+14xPP7-GAL10
5.6 kb
4.0 kb
2.3 kb
*
*
GAL10
ncRNA
<
TUB1
C
glu n = 3 exp (51,626 cells)
raf n = 3 exp (159,592 cells)
Probability
RNA per cell
E
1/c, mean transcription interval (min)
FISH glu
FISH raf
live-cell
D
FISH on PP7 (GAL10 ncRNA)
Poisson model, fit:
cT = 0.08 ± 0.01 mean # RNAs at the TS
n = 98,336 cells
raf
Probability
RNAs per transcription site
F
autocorrelation from individual traces
autocorrelation from average trace
corrected autocorrelation
G(t)
Time lag (s)
G
FISH on MS2 (GAL10)
Live cell
Poisson model
Bursting model, fit:
n = 1.9 RNAs/burst
aT = 4.2 bursts/dwell time
Probability
RNAs per transcription site
H
Measured GAL10 traces
Simulated traces with
n=1.9, a=1.9/min, T=133s
# nascent RNAs
Time (min)

Fig. S2 A

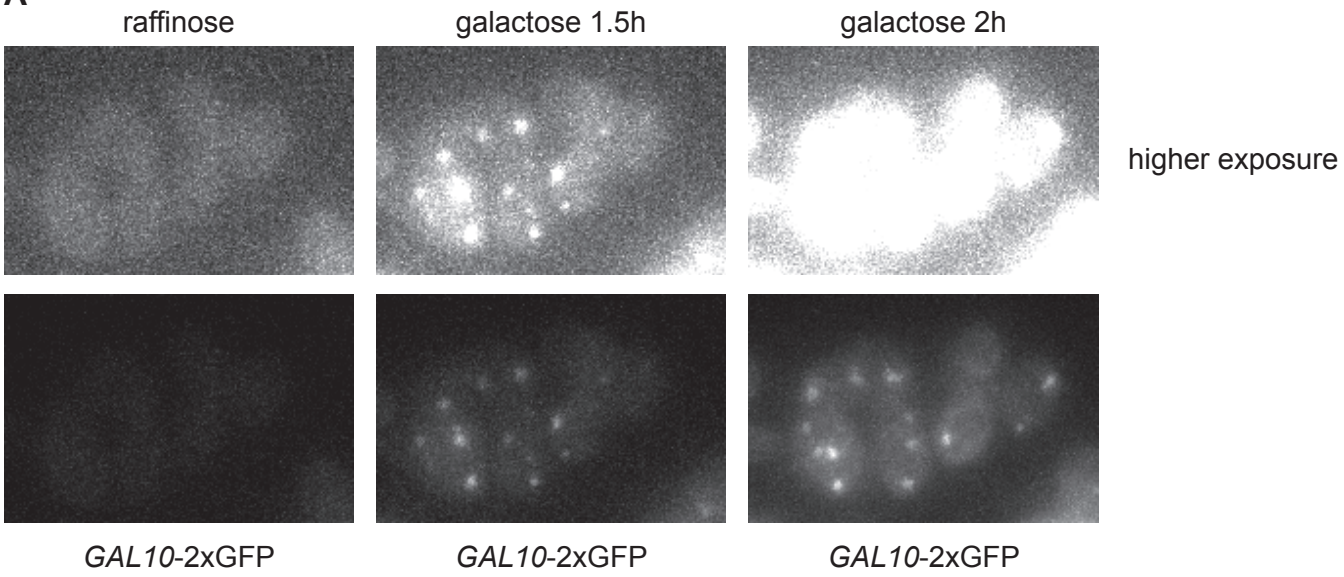
raffinose
galactose 1.5h
galactose 2h
higher exposure
GAL10-2xGFP
GAL10-2xGFP
GAL10-2xGFP

B

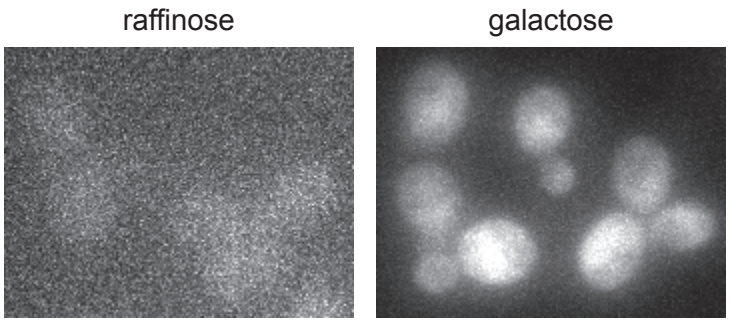
raffinose
galactose
*gal10*Δ::2xGFP
*gal10*Δ::2xGFP

Fig. S3

A

$$\frac{d[G1]}{dt} = \alpha_{0G1} + \alpha_{gal}\varepsilon + \frac{\alpha_{G1}[G4]^3}{[G4]^3 + K_{G1}^3} + \omega[G1][G80] - \gamma_{G1}[G1]$$

$$\frac{d[G3]}{dt} = \alpha_{gal} + \frac{\alpha_{G3}[G4]^2}{[G4]^2 + K_{G3}^2} + \delta[G3][G80] - \gamma_{G3}[G3]$$

$$\frac{d[G4]}{dt} = \alpha_{G4} + \beta[G80][G4] - \gamma_{G4}[G4]$$

$$\frac{d[G80]}{dt} = \alpha_{0G80} + \frac{\alpha_{G80}[G4]^2}{[G4]^2 + K_{G80}^2} + \omega[G1][G80] + \delta[G3][G80] + \beta[G80][G4] - \gamma_{G80}[G80]$$

B

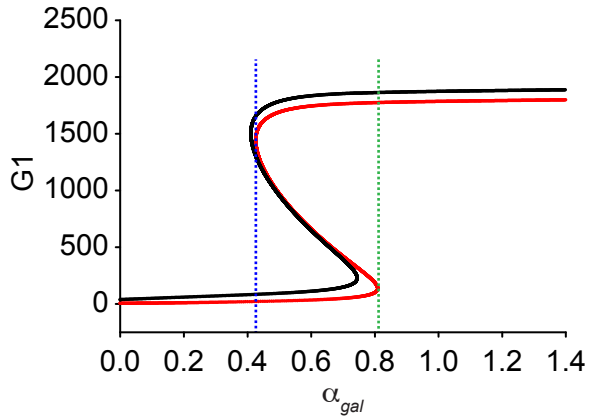

C

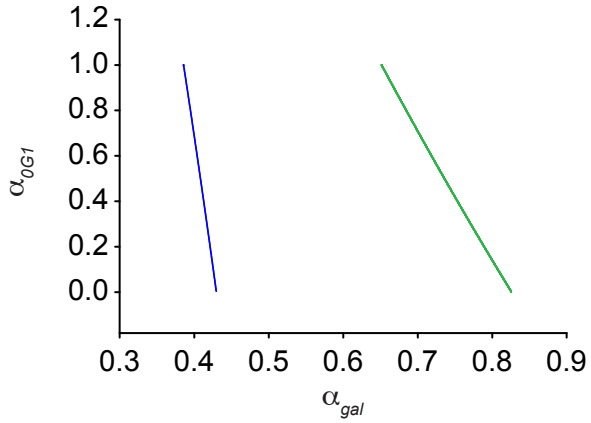

Fig. S4

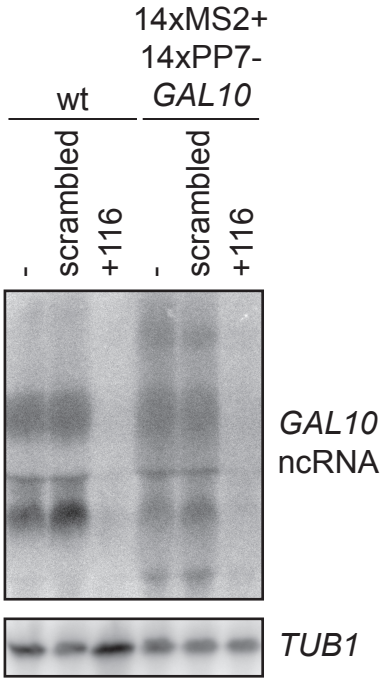
wt
14xMS2+
14xPP7-
GAL10
-
scrambled
+116
-
scrambled
+116
GAL10
ncRNA
TUB1

Supplemental figure legends

Figure S1. Measuring *GAL10* and *GAL10 ncRNA* transcription in live yeast cells. Related to Fig. 1. (A) Northern blot of *GAL10* in wildtype BY4743 and the MS2+PP7 tagged *GAL10* strain, after 30 minutes galactose induction. The tagged copy of *GAL10* is indicated with an asterisk(*). Compared to wt total levels of *GAL10* are 1.2 fold increased (± 0.19) after 30 minutes of galactose induction (B). Northern blot of *GAL10* ncRNA in wildtype BY4743 and the MS2+PP7 tagged *GAL10* strain, grown in raffinose. The tagged transcripts are indicated with asterisks (*). The tagged strain also displays a shorter additional transcript, marked with <. Compared to wt, total levels of ncRNA are 1.8 fold increased in raffinose (± 0.13) (C) Distribution of the number of *GAL10* ncRNA per cell as measured by smFISH in glucose and in raffinose. Data is from three experiments with the total number of cells analyzed indicated. (D) TS intensity was normalized with the intensity of single cytoplasmic ncRNA. The distribution of the number of *GAL10* ncRNA transcripts at the TS fits a Poisson model of transcription initiation. The fit of cT (initiation * dwell time) of one experiment in raffinose with the highest cell number is shown. The fit of 3 experiments is 0.08 ± 0.01 average number of RNA at the TS (E) Mean interval between *GAL10* ncRNA transcription events, 1/c (1/initation rate). The FISH data in raffinose and glucose is acquired by fitting the transcription site intensity from 3 smFISH experiments, as in (D), and using a dwell time of 93.5 s (Fig 1E). The live cell measurement is from Fig. 1F (F) The blue curve shows the autocorrelation of *GAL10* transcription site intensities from the individual traces. Because of non-steady-state effects, there is a long tale. To correct for this, the traces are all aligned on the start of *GAL10* transcription, and averaged. The black curve indicates the autocorrelation from the average trace. The corrected autocorrelation (red) is acquired by subtracting the black curve from the blue curve. (G) The distribution of number of RNAs per transcription site, normalized by the intensity of single cytoplasmic RNAs, as measured by smFISH after 30 min of galactose induction, fits a bursting model (black), but not a Poisson model (purple) of transcription initiation. The FISH data was used to scale the fluorescence intensity of the live cell data around 30 minutes to number of RNAs (blue). Examples of resulting traces are shown in (H) and Figure 1G. The scaled live-cell data reproduces shape of the smFISH distribution, supporting our approach. (H) The low burst size was surprising, because it appears to contradict the high fluorescent intensity found at the TS. However, the indicated parameters were used to simulate TS traces, which yielded highly similar transcription patterns as the measured traces. On the left are examples of measured *GAL10* traces, scaled by smFISH, and on the right are examples of simulated traces with the parameters indicated. The patterns are highly similar, indicating that the parameters are likely close to the true values. Even though the average burst contains only 2 polymerases, the high frequency results in an average occupancy of *GAL10* of around 8 polymerases. Moreover, it is not uncommon to have more than 20 polymerases on the gene at the same time.

Figure S2. Localization of GAL10-2xGFP in punctate spots. Related to Fig. 4. (A) *GAL10*-2xGFP expressing in raffinose and after galactose induction. The top images are the same as the bottom images with higher exposure. In un-induced conditions no fluorescence is observed, but after galactose exposure, Gal10p-2xGFP is localized to several punctate spots. Although surprising, there are several indications that this may be the correct localization of Gal10p. First, deletion of the coding region of *GAL10* abrogates the spot-like localization (see B), indicating the punctate localization is not an artifact of overexpressing 2xGFP. Second, Gal10p-2xGFP is fully functional and can support growth on galactose plates as the sole copy. Third, a similar localization was previously observed for Gal7p (Christacos et al., 2000). (B) Cellular fluorescence

of *gal10*Δ-2xGFP cells in raffinose and galactose. Note that the punctate pattern of *GAL10* disappears if the *GAL10* ORF is removed.

Figure S3. Computational model of transcriptional leakage in the galactose network. Related to Fig. 6. (A) Coupled nonlinear ordinary differential equation description of the galactose network from Venturelli et al., 2012. The model contains an additional leakage rate α_{0G1}. This model exhibits bistability and hysteresis as observed in the experimental data. (B) Steady state behavior of the model for two values of α_{0G1} (CRIPSRi scrambled: red, α_{0G1}=0.13; CRISPRi +116: black, α_{0G1}=0.65). The steady state curves have the classic reverse "s" shape for bistability and hysteresis. The bistable region is delimited by two limit points, indicated on the wt red bifurcation graph as blue and green dotted lines. A 5-fold increase in the leakage rate α_{0G1} results in a rightward shift of the right limit point (jump up point) but less of a shift of the left limit point (jump down point). (C) Limit point values as a function of leakage rate (α_{0G1}). Left limit point (jump down point): blue curve; right limit point (jump up point): green curve. α_{0G1} is plotted as the ordinate (instead of abscissa) for easier comparison to panel B.

Figure S4. Northern blot of *GAL10* ncRNA in strains with and without CRISPRi. Related to Fig. 7. The MS2+PP7 tagged *GAL10* strain shows an additional *GAL10* ncRNA transcript compared to wildtype, but all transcripts disappear in the strain with CRISPRi +116.

Supplemental movie legends

Movie S1. *GAL10* ncRNA is present at the TS for several frames. Related to Fig. 1. Time-lapse movies of *GAL10* ncRNA transcription in raffinose (Fig. 1D), imaged with 30s interval and 150 ms exposure using a custom built wide-field microscope. The images show maximum intensity projections of 9 *z*-planes (left), and side-views (right and bottom) with no further image processing. The tracking of the TS is indicated by a blue cross.

Movie S2. *GAL10* shows transcriptional bursting, with periods of transcriptional activity followed by periods of inactivity. Related to Fig. 1. Time-lapse movies of *GAL10* transcription after addition of 2% galactose (Fig. 1G), imaged with 30s interval and 150 ms exposure. The images show maximum intensity projections of 9 *z*-planes (left), and side-views (right and bottom) with no further image processing. The tracking of the TS is indicated by a blue square.

Movie S3. Example of a cell showing *GAL10* ncRNA transcription before *GAL10* transcription. Related to Fig. 2. Time-lapse movies of *GAL10* ncRNA (green, left) and *GAL10* (red, middle) transcription and the merge of both signals (right) after addition of 2% galactose (Fig. 2A), imaged with 30s interval and 150 ms exposure. For each color, the images show maximum intensity projections of 9 *z*-planes (left), and side-views (right and bottom) with no further image processing. The tracking of the TS is indicated by a blue cross or a blue square.

Movie S4. Example of a cell showing *GAL10* ncRNA and *GAL10* transcription simultaneously. Related to Fig. 2. Time-lapse movies of *GAL10* ncRNA (green, left) and *GAL10* (red, middle) transcription and the merge of both signals (right) after addition of 2% galactose (Fig. 2B), imaged with 30s interval and 150 ms exposure. For each color, the images show maximum intensity projections of 9 *z*-planes (left), and side-views (right and bottom) with no further image processing. The tracking of the TS is indicated by a blue cross or a blue square.

Table S1. Yeast strains used in this study. Related to Experimental Procedures. This table includes the name, genotype and source of the strains used in this study.

Name	Genotype	Source
BY4741	*MATa his3Δ1 leu2Δ0 met15Δ0 ura3Δ0*	Brachmann et al., 1998
BY4743	*MATa/α his3Δ1/his3Δ1 leu2Δ0/leu2Δ0 LYS2/lys2Δ0 met15Δ0/MET15 ura3Δ0/ura3Δ0*	Brachmann et al., 1998
YTL048	*as BY4743, GAL10/14xMS2(sense)+14xPP7(antisense)-GAL10*	this study
YTL117	*YTL048 with pTL041 and pTL042*	this study
YTL180	*as BY4741, GAL10-2xGFP::loxP-kanMX6-loxP*	this study
YTL181	*YTL180 with pTL044 and pTL053*	this study
YTL182	*YTL180 with pTL044 and pTL055*	this study
YTL133	*BY4743 with pTL044 and pTL051*	this study
YTL134	*BY4743 with pTL044 and pTL053*	this study
YTL135	*BY4743 with pTL044 and pTL054*	this study
YTL136	*BY4743 with pTL044 and pTL055*	this study
YTL155	*BY4743 with pTL044 and pTL061*	this study
YTL189	*BY4741 with pTL044 and pTL053*	this study
YTL190	*BY4741 with pTL044 and pTL055*	this study
YTL138	*YTL048 with pTL044 and pTL053*	this study
YTL140	*YTL048 with pTL044 and pTL055*	this study
YTL226	*YTL048 with pTL044 and pTL053 and pTL042*	this study
YTL227	*YTL048 with pTL044 and pTL055 and pTL042*	this study
YTL183	*as BY4741, gal3Δ::kanMX6*	Open Biosystems
YTL187	*YTL183 with pTL044 and pTL055*	this study
YTL188	*YTL183 with pTL044 and pTL053*	this study
YTL219	*as BY4741, gal4Δ::kanMX6*	Open Biosystems
YTL220	*YTL219 with pTL044 and pTL055*	this study
YTL221	*YTL219 with pTL044 and pTL053*	this study
FY4	*MATa, ura3-52, trp1-Δ63, his3-Δ200, leu2::PET56*	Houseley et al., 2008
MMY160	*as FY4, GAL10-Reb1-BSΔ URA3::pMV12 (EcoRI/Xho1 - Reb1 BSΔ)*	Houseley et al., 2008
FM1282	*MATa lys2Δ0 ura3Δ0 THD3pro-eGFP-cyc1term*	Hittinger and Carroll, 2007
FM1283	*MATa lys2Δ0 ura3Δ0 THD3pro-eGBP-cyc1term*	Hittinger and Carroll, 2007
YTL305	*FM1282 with leu2::hphMX, pTL044 and pTL055*	this study
YTL306	*FM1282 with leu2::hphMX, pTL044 and pTL053*	this study
YTL307	*FM1283 with leu2::hphMX, pTL044 and pTL055*	this study
YTL308	*FM1283 with leu2::hphMX, pTL044 and pTL053*	this study
YTL312	*FM1282 with pTL078*	this study
YTL313	*FM1282 with pTL077*	this study

YTL314	*FM1283 with pTL078*	this study
YTL315	*FM1283 with pTL077*	this study

Table S2. Plasmids used in this study. Related to Experimental Procedures. This table includes the name, description and source of the plasmids used in this study.

Name	Description	Source
pTL032	14x MS2 sense + 14x PP7 antisense with loxP-kanMX-loxP	this study
pTL014/ pSH47	pURA P_{GAL} *CRE* recombinase	T.S. Karpova
pTL041	pURA P_{ADE3} PCP-NLS-2xGFP	this study
pTL042	pHIS P_{MET17} MCP-NLS-mKate2	this study
pTL044/ pSLQ1501	pLEU cas9 caspase dead	M.H. Larson/ J.S. Weissman
pTL051	pURA guide RNA *GAL10* ncRNA TATA (AGTTTGGAAATGGTATATAA)	this study
pTL053	PURA guide RNA *GAL10* ncRNA +116 (CATGCTGATAGATAATGAGA)	this study
pTL054	pURA guide RNA *GAL10* ncRNA +1534 (GTTTTGGTTACAGGTGGTGC)	this study
pTL055	pURA guide RNA scrambled/control (AGGTACGTACTGTAAGTTAA)	this study
pTL061	pURA guideRNA *GAL10* ncRNA +123 template strand (ATCTATCAGCATGTACTCGG)	this study
pTL077	pURA P_{ADE3} *GAL1*	this study
pTL078	pURA empty vector	this study

Table S3. Oligos used in this study. Related to Experimental Procedures. This table includes the oligo number, name, sequence and purpose of the oligos used in this study.

Oligo #	Name	Sequence	Purpose
297	GAL10-5'-F	TATTAAACTTCTTTGCGTCCATCCAAAAAAAAAGTAAGAATT TTTGAAAATTCAATATAACCGCTCTAGAACTAGTGGATCC	Construction YTL048
298	GAL10-5'-R	AGCACCACCTGTAACCAAAACAATTTTAGAAGTACTTTCACT TTGTAACTGAGCTGTCATGCATAGGCCACTAGTGGATCTG	Construction YTL048
842	GAL10-Cterm-tag-F	GATTGTGTAACCTTGAAAAACGGTGAAACTTACGGGTCCAA GATTGTCTACAGATTTTCCGCTCTAGAACTAGTGGATCC	Construction YTL180
843	GAL10-Cterm-tag-R	GCAATTAAGAACTAAAAGATATAGAGTGCATATTTTCAAGAA GGATAGTAAGCTGGCAAAGCATAGGCCACTAGTGGATCTG	Construction YTL180
552	GAL10-F1	GGCTGTAGGTGAATCTACAC	Northern blot
553	GAL10-R1	ATACCTAGCGGATCTTCTCC	Northern blot
597	GAL10-R1-2	TTAATCCAGAGGGATGTGCG	Northern blot
555	GAL10-F2	ATTTGAAGGTTTGTGGGGCC	Northern blot
556	GAL10-R2	GTGGAAATGTAAAGAGCCCC	Northern blot
557	GAL10-F2-2	TTATTGTTCGGAGCAGTGCG	Northern blot
924	GAL1-F1	CCTGAGTTCAATTCTAGCGC	Northern blot
926	GAL1-R1	AGAGTGAGCAACATGGAGAC	Northern blot
927	GAL1-R1-2	CAACGGCAAATCGAACTTCC	Northern blot
598	TUB1-F1	CGTTCCAAGGGCTATTTACG	Northern blot

			/qPCR
599	TUB1-R1	GAAGTAGACACTTGTGGAGC	Northern blot
600	TUB1-R1-2	TACGGCAAATTCCAGCTTGG	Northern blot /qPCR
822	GAL10-F3	ACAAAGCCAACGGTCTTAGG	qPCR
824	GAL10-R3-2	TTGGACCCGTAAGTTTCACC	qPCR

Table S4 Fitted Hill function parameters to data. Related to Experimental Procedures. This table includes the fitted Hill function parameters computed with the function nls in the open software tool R (http://www.r-project.org/)

	h	k
Galactose scrambled	4.954	0.00190
Galactose +116	4.789	0.00190
Raffinose scrambled	8.207	0.00418
Raffinose +116	7.505	0.00370

Supplemental Experimental Procedures

Analysis of transcriptional time traces

Maximum intensity projections were computed. The intensity of the TS was calculated for each color separately by fitting a 2D Gaussian mask after local background subtraction using custom IDL software as described previously (Coulon et al., 2014; Larson et al., 2011). If no spot was found above a band-pass threshold, the previous location was used to measure the intensity for *GAL10*, while the signal was set to 0 for *GAL10* ncRNA.

Cells that were incubated in galactose for extended time periods showed depletion of coat protein from the nucleus as a result of the high mRNA production, making the TS invisible. Because of this nuclear depletion of coat proteins, nascent GAL10 RNAs became undetectable typically after a few bursts (Fig. 2C). Hence the traces were trimmed after the last detected burst. Traces were then rescaled from arbitrary fluorescence units to number of nascent RNAs so that the distribution of values at 30 min of induction matches that of the smFISH experiment, also performed at 30 min of induction (Fig. S1G). To align time traces (Figs. 2D and 7C), we identified the first occurrence of GAL10 transcription using a threshold of 3.5 standard deviations above background. Average trace plots (Figs. 2D and 7C) were obtained by taking, for each time point, the mean of all aligned traces that are not trimmed at that particular time point. Autocorrelation functions were computed and averaged as described previously (Coulon et al., 2014) with minor modifications to account for the non-stationary nature of the time traces (manuscript in preparation). Briefly, in order to reveal the dynamics of single bursts, we removed the slow component reflecting the non-stationarity of the induction process (i.e. the fact that the gene always start inactive and turns on during the course of the acquisition) by subtracting the autocorrelation function of the average aligned trace (Fig. 2D) from the average autocorrelation function of all the traces (Fig. S1F). This yields an autocorrelation that only has two components: a slow one reflecting the coat protein depletion and the trimming process (i.e. highly dependent on technical factors such as initial coat protein levels), and a fast one reflecting the bursting dynamics (consistent between experimental replicates). The shape of the fast component reveals the kinetics of bursting (manuscript in preparation). In particular, its linear nature indicates that initiations occur in short bursts that are significantly shorter than the dwell time of the nascent RNAs at the locus (i.e. elongation + termination times). This RNA dwell time is given by the intersection of the fast and slow linear components.

Analysis of single-molecule FISH

Spots were localized using custom IDL software, as described previously (Coulon et al., 2014). Cell and nuclear outlines were determined with Cell Profiler (Carpenter et al., 2006). TS were defined as nuclear spots, and were normalized to the fluorescent intensity of cytoplasmic RNAs. The TS distribution was fit with a Poisson distribution or a random telegraph model (Raj et al., 2006).

Competition assay

Competition experiments we performed as in (Hittinger and Carroll, 2007), with minor modifications. For glucose experiments, overnight cultures of BFP and GFP cells were mixed around 50% and grown for 24h in selective media with 2% glucose. The percentage of GFP was measured by flow cytometery (GFPstart). The culture was diluted and grown for another 24h, after which the percentage of GFP positive cells was measured again (GFPend). For galactose or mixed conditions, O/N cultures were mixed around 50% and grown for 24h in selective media with 2% raffinose. After measuring GFPstart, the cells were put in various media conditions (2%

galactose, 2% glucose + 2% galactose or 0.02% glucose + 0.01% galactose + 2% raffinose) for 24h, after which GFPend was measured. Because the fitness defect of ncRNA inhibition was small, to get reliable numbers cells were diluted and grown for another 24h (48h total) before GFPend was measured. All experiments were done with dye swaps. Fig. 5I represent 7 measurements for each condition (3 empty vector (ev) vs ev and 4 *GAL1*-expressing plasmid versus ev in 2 dyeswaps). Fig. 5J represents 8 measurements for glucose (4 scr vs scr, 4 +116 vs scr) and 16 measurements for galactose, and the mixed conditions (8 scr vs scr, 8 +116 vs scr). Only living cells were used to determine the GFP percentage, by staining the cells with propidium iodide and selecting for non-stained cells. For all experiments, $2*10^5$ were measured. The fitness defect was calculated similarly to (Hittinger and Carroll, 2007), without normalizing for the control.

RNA-seq

RNA from mid-log yeast cultures grown in glucose was isolated by phenol extraction. RNA was cleaned with Qiagen RNAeasy columns including DNAse treatment. Two replicates of BY4741 containing Cas9d and guideRNAs for scrambled and +116 were sequenced on one HiSeq2500 lane using Illumina TruSeq v4 chemistry. Sample yields ranged from 84 to 105 million pass filtered reads. After trimming the reads of adapters and low quality bases using Trimmomatic software, they were aligned using Tophat software to the yeast (Ensembl_YeastS288C_EF4) reference genome modified to contain three CRISPR plasmid sequences. Between 81% and 84% of reads aligned to the reference genome and between 76% and 79% mapped uniquely. The ratio of uniquely mapped reads was used to normalize the reads in Fig. 6B. Data was analyzed using a Bioconductor workflow (http://www.bioconductor.org/help/workflows/rnaseqGene/) based on the R packages GenomicAlignments and DESeq2 (Lawrence et al., 2013; Love et al., 2014). Fig. 6C was generated by exporting the normalized reads from DESeq2. Fig.6D-F were generated using the plotMA function of DESeq2.

Modeling of the GAL network

In order to confirm our experimental observation that ncRNA plays a role in suppressing transcriptional leak of *GAL10*, we considered the mathematical model of the galactose regulatory system of Venturelli et al., 2012 (Fig. S3A), where we have added a leakage rate α_{0G1}. In all of our analysis, we use the exact same parameters as Venturelli et al. except that we set α_{G1} to 7, the reason of which we discuss below. We also introduced heterogeneity between cells, because the theoretical dose response of a single cell (or a population of cells with identical initial conditions) shows switch-like behavior in transitioning from low galactose to high galactose (Fig. S3). In contrast, the measured sigmoidal population dose response is the superposition of many individual cell responses. By allowing for heterogeneity in the synthesis rate of the activator Gal4p one obtains a distribution of responses whose sum is the population response (Fig. 6A).

Our data shows that G1 is a surrogate for *GAL10*. The model exhibits bistability and hysteresis as observed in the data. As seen in Fig. S3B, the model steady state as a function of galactose (α_{gal}) has the classic reverse "S" shape indicative of bistability and hysteresis. The bistable region is delimited by two limit points. In the bistable region, cells are either uninduced (lower branch) or induced (upper branch). For galactose level less than then left limit point, all

cells are on the lower branch. They will remain on the lower branch as galactose is increased until galactose reaches the right limit point whereupon cells will become activated and transition to the upper branch. Conversely, if cells started on the upper branch and galactose was lowered, they would remain on the upper branch. This mirrors the data as seen in Fig. 4, where the dose response of cells pretreated with raffinose are positioned at higher levels of galactose compared to those pretreated with galactose.

We first asked whether the width of the bistable region in the model matched the data. We were unable to directly convert the units of α_{gal} (nM/min) in the model to experimental units since we were unable to quantify how much galactose in the cell culture medium entered each particular cell. Hence, we asked whether the ratio of the position of the left limit point to the right limit point matched the ratio of the EC50 of the galactose pretreated cells to the raffinose pretreated cells. We found that the original parameters of the Venturelli et al. model did not quite match this ratio. However, by reducing the *GAL4* to *GAL1* feedback parameter α_{G1} to 7 nM*min^{-1} from its original 15 nM*min^{-1}, the model quantitatively matched the data. This concordance is quite remarkable, and any small differences may be due to strain and/or experimental variability. We thus used $\alpha_{G1} = 7$ nM*min^{-1} in all of our analysis.

The data showed that blocking *GAL10* ncRNA (+116) resulted in 5-7 fold increase in *GAL10* leak rate and an 11% leftward shift of the dose response curve for cells pretreated in raffinose but no observable shift in the dose response for cells pretreated in galactose. We tested this in the model by seeing how a fold increase in the G1 baseline leak rate affected the positions of the left and right limit points, which are surrogates of the EC50s of the dose response curves. Fig. S3B, shows that with a fivefold increase in leak rate the steady state curves of the model shifts left, with the right limit point shifting much more than the left limit point in accordance with the experiments.

This observation is quantified directly in Fig. S3C, where we use continuation software (XPPAUT, http://www.math.pitt.edu/~bard/xpp/xpp.html) to follow the position of the two limit points (in units of α_{gal}) as a function of G1 leak rate α_{0G1}. The left limit point is well fit by the function $\alpha_{gal} = -0.0039\alpha_{0G1} + 0.43$ and the right limit point is well fit by the function $\alpha_{gal} = -0.1743\alpha_{0G1} + 0.8237$. The slope of the right limit point is nearly forty times greater than the left, which means that the right limit point is forty times more sensitive to changes in leak rate than the left limit point. We explicitly checked to see if the change in limit point position quantitatively matched the change in EC50 in the data by seeing if there existed a G1 leak rate α_{0G1} such that a 5 - 7 fold increase in leak resulted in the experimentally observed shifts. In particular, it must show that the raffinose pretreated cells would shift by approximately 11% under +116 while the galactose pretreated cells would show no observable shift. The expected scrambled α_{0G1} is given by the formula

$$\alpha_{0G1} = \frac{bS}{a\left(f-1+S\right)} \pm \left|1 - \frac{S}{f-1+S}\right| \frac{bC}{a\left(f-1+S\right)} \qquad \text{Eqn. S1}$$

where $S \pm C$ is the fractional shift and uncertainty of the limit point, the limit point obeys the function $\alpha_{gal} = -a\alpha_{0G1} + b$, and *f* is the fold increase in leak rate between the scrambled and +116 conditions.

If we observed a shift in the EC50 for the raffinose pretreated cells of *S* = 0.11 with uncertainty *C* of 0.02 and take *f* = 5 then this formula yields α_{0G1} = 0.13 ± 0.02 nM*min^{-1}. We now check to see if this predicted leak rate is below the predicted threshold for detection for the galactose pretreated cells. If we assume that the resolution on the shift in the EC50 of the galactose pretreated dose response curve is *r* then the upper bound on α_{0G1} is given by

$$\alpha_{0G1} < \frac{0.43r}{0.0039(4+r)} \approx 27r \qquad \text{Eqn. S2}$$

Any baseline leak rate that is larger than this bound would have been detectable in the experiment. For an *r* of 0.82% this amounts to an upper bound of $\alpha_{0G1} \approx 0.22$. This implies that the Venturelli et al. model, with the introduction of a leak rate and a change in just one parameter is fully consistent with the hypothesis that ncRNA represses *GAL10* transcriptional leak rate.

The dose response curves in Fig. 4 for the fraction of induced cells as a function of galactose concentration obtained from the FACS data were well fit by Hill functions $x^h / \left(EC_{50}^h + x^h\right)$ with parameters in Table S4. However, for a fully deterministic bistable system, the dose response curves would be infinitely sharp as cells would go from an inactive state to being fully active once α_{gal} exceeded the right limit point if the system were initially on the lower branch or conversely go from a fully active to an inactive state once α_{gal} dropped below the left jump down point, if initially on the upper branch. This would imply an infinite Hill coefficient *h*, which does not match the data.

We can resolve this discrepancy if we assume that cells are heterogeneous, i.e. the parameters of the model may vary between cells. As an example, we suppose that the baseline transcription rate for G4 differs from cell to cell. This results in different baseline G4 values or different initial conditions for each run. We implement this by assuming that the baseline rate α_{G4} is normally distributed with mean 0.2 nM*min^{-1} as specified by Venturelli. Figure 6H (red dashed line) shows model generated dose response curves (generated in the software tool R) for parameters α_{G1} = 7 nM*min^{-1}, α_{0G1} = 0.13 nM*min^{-1}, $SD(\alpha_{G4})$ = 0.065 nM*min^{-1}. We have scaled α_{G1} such that the EC_{50} for the galactose scrambled conditions match the data. The model dose response curves are given by the fraction of active cells at a given α_{gal} with initial condition given by the steady state of the model for α_{gal} equal to zero for the raffinose pretreated condition and 2 for the galactose pretreated condition. The curves were given by averages over 400 samples and did not noticeably change with more samples. The model fits remarkably well even though the parameters were not optimized for best fit.

Supplemental references

Brachmann, C.B., Davies, A., Cost, G.J., Caputo, E., Li, J., Hieter, P., and Boeke, J.D. (1998). Designer deletion strains derived from Saccharomyces cerevisiae S288C: a useful set of strains and plasmids for PCR-mediated gene disruption and other applications. Yeast Chichester Engl. *14*, 115–132.

Carpenter, A.E., Jones, T.R., Lamprecht, M.R., Clarke, C., Kang, I.H., Friman, O., Guertin, D.A., Chang, J.H., Lindquist, R.A., Moffat, J., et al. (2006). CellProfiler: image analysis software for identifying and quantifying cell phenotypes. Genome Biol. *7*, R100.

Christacos, N.C., Marson, M.J., Wells, L., Riehman, K., and Fridovich-Keil, J.L. (2000). Subcellular localization of galactose-1-phosphate uridylyltransferase in the yeast Saccharomyces cerevisiae. Mol. Genet. Metab. *70*, 272–280.

Coulon, A., Ferguson, M.L., de Turris, V., Palangat, M., Chow, C.C., and Larson, D.R. (2014). Kinetic competition during the transcription cycle results in stochastic RNA processing. eLife *3*.

Hittinger, C.T., and Carroll, S.B. (2007). Gene duplication and the adaptive evolution of a classic genetic switch. Nature *449*, 677–681.

Larson, D.R., Johnson, M.C., Webb, W.W., and Vogt, V.M. (2005). Visualization of retrovirus budding with correlated light and electron microscopy. Proc. Natl. Acad. Sci. U. S. A. *102*, 15453–15458.

Larson, D.R., Zenklusen, D., Wu, B., Chao, J.A., and Singer, R.H. (2011). Real-time observation of transcription initiation and elongation on an endogenous yeast gene. Science *332*, 475–478.

Lawrence, M., Huber, W., Pagès, H., Aboyoun, P., Carlson, M., Gentleman, R., Morgan, M.T., and Carey, V.J. (2013). Software for Computing and Annotating Genomic Ranges. PLoS Comput Biol *9*, e1003118.

Love, M.I., Huber, W., and Anders, S. (2014). Moderated estimation of fold change and dispersion for RNA-seq data with DESeq2. Genome Biol. *15*, 550.

Raj, A., Peskin, C.S., Tranchina, D., Vargas, D.Y., and Tyagi, S. (2006). Stochastic mRNA synthesis in mammalian cells. PLoS Biol. *4*, e309.

Venturelli, O.S., El-Samad, H., and Murray, R.M. (2012). Synergistic dual positive feedback loops established by molecular sequestration generate robust bimodal response. Proc. Natl. Acad. Sci. U. S. A. *109*, E3324–E3333.